ACS APPLIED NANO MATERIALS

Article

Cite This: ACS Appl. Nano Mater. 2018, 1, 5451−5459

www.acsanm.org

Multisite Inhibitors for Enteric Coronavirus: Antiviral Cationic Carbon Dots Based on Curcumin

Du Ting,[†] Nan Dong,[‡] Liurong Fang,[‡] Jian Lu,[†] Jing Bi,[‡,§] Shaobo Xiao,*[,‡,⊥] and Heyou Han*[,†,⊥]

[†]State Key Laboratory of Agricultural Microbiology, College of Food Science and Technology, College of Science, and [‡]State Key Laboratory of Agricultural Microbiology, College of Veterinary Medicine, Huazhong Agricultural University, Wuhan 430070, P. R. China

[§]Department of Immunology and Aetology, College of Basic Medicine, Hubei University of Chinese Medicine, Wuhan 430065, P. R. China

S *Supporting Information*

ABSTRACT: The research of carbon-based antivirals is still in its infancy, and their development into safe and effective carbon dots (CDs) with antiviral activity at multiple points in the life cycle of the virus remains to be explored. Here, we report a one-step method to apply curcumin in order to prepare of uniform and stable cationic carbon dots (CCM-CDs) with antiviral properties. The inhibitory effect of CCM-CDs on viral replication was studied by using porcine epidemic diarrhea virus (PEDV) as a coronavirus model. PEDV is applied as a coronavirus model to study the antiviral effect of as-prepared CCM-CDs on its replication. The cationic CCM-CDs treatment is found obviously to inhibit the proliferation of PEDV compared with the common CDs (EDA-CDs). The CCM-CDs treatment can change the structure of surface protein in viruses, thereby inhibiting viral entry. It can also suppresses the synthesis of negative-strand RNA of the virus, the budding of the virus, and the accumulation of reactive oxygen species by PEDV. Furthermore, CCM-CDs treatment is also found to suppress viral replication by stimulating the production of interferon-stimulating genes (ISGs) and proinflammatory cytokines. These results offer theoretical support for the development of CCM-CDs as a hopeful antiviral drug for the treatment of coronavirus infections, including PEDV.

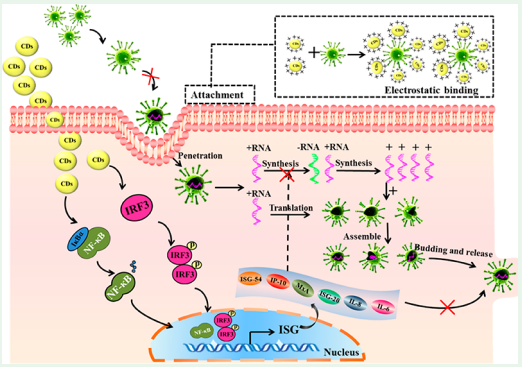

KEYWORDS: *curcumin, carbon dots, antiviral, interferon-stimulating genes, proinflammatory cytokines*

1. INTRODUCTION

Curcumin (CCM) is a polyphenol compound obtained from turmeric roots. Because of its antioxidant, antiviral, anti-inflammatory, anticancer, antibacterial functions, and so on, potential applications of CCM in multiple industries are gaining interest.[1−3] Mouler Rechtman et al. demonstrated that CCM inhibited the expression and multiplication of the hepatitis B virus by downregulating PGC-1α.[4] Ali and Banerjea found that CCM inhibited human immunodeficiency virus (HIV)-1 infection by facilitating the degradation of Tat protein and reducing Tat-mediated transcription of the toll-like receptor promoter.[5] Narayanan et al. evaluated the antiviral activity of CCM against Rift Valley fever virus (RVFV). The mechanism confirmed that CCM inhibited RVFV replication by preventing phosphorylation of ISK-β NSs protein in the NF-κB pathway.[6] However, the pure CCM cannot be widely applied because of its insolubility in physiological media and poor bioavailability in vivo. To overcome these shortcomings of CCM, a widely used strategy is to encapsulate CCM in inorganic-based carriers,[7,8] but the process of synthesizing these nanoparticles is relatively tedious and time-consuming; furthermore, this treatment does not significantly improve the antiviral activity of CCM. Thus, developing a simple, safe, and effective method to improve the bioavailability, solubility, aand antiviral activity is extremely important.

Because of their different compositions and characteristics, nanoparticles can be perfectly used as a carrier in the efficient delivery of drugs to special sites.[9,10] Besides, nanoparticle-based antiviral agents have been reported as potential alternatives in the treatment of diseases because of their distinctive biological properties derived from morphological (e.g., size, structure) and physicochemical features, different from those of traditional small-molecule drugs.[11,12] Antiviral nanomaterials, such as silver nanoparticles (AgNPs), functional gold nanoparticles,[13,14] peptide,[15] and polyvalent nanoarchitectures,[16−18] have aroused widespread research interest.[19] Among the nanomaterials, AgNPs have the highest potential for commercialization, and numerous studies have demonstrated that AgNPs possess strong antiviral activity against HIV, H1N1 influenza virus, herpes simplex virus, and so on.[20,21] The complicated antiviral mechanisms of AgNPs include competing viruses binding to cells, interactions with DNA, attachment to the cell surface to

Received: May 11, 2018
Accepted: September 12, 2018
Published: September 12, 2018

DOI: 10.1021/acsanm.8b00779
ACS Appl. Nano Mater. 2018, 1, 5451−5459

change the membrane characteristics, and inactivation of virus particles before entry and enzyme damage.[22] However, before the adhibition of metal nanoparticles to therapeutic or preventive therapy, it is essential to assess their cytotoxicity to most human cells and the underlying long-term sequelae caused by contact with these compounds.[23,24] Therefore, nano-antibiotics based on nonmetallic nanoparticles have attracted widespread attention because of their outstanding antiviral characteristics. Recently, carbon-based nanomaterials have been confirmed to have potent antiviral properties.[25−27] Sametband et al. found that graphene oxide derivatives could suppress viral infection by competing for virus−cell binding.[28] Barras et al. investigated that surface-functionalized carbon nanodots could function as entry inhibitors through interaction with the virus at the early stage of a viral infection. Meanwhile, our previous work has demonstrated that carbon dots (CDs) might inhibit viral replication by positively regulating the antiviral type I interferon (IFN) response.[29] In this study, novel CDs from CCM as the precursor were prepared, which could improve the bioavailability of CCM and achieve a synergisic antiviral effect.

In the present study, it is reported that antiviral cationic carbon dots (CCM-CDs) are prepared from herbs for the first time, and this provides novel clues to improve the antiviral activity of herbs. We find that CCM-CDs treatment can significantly inhibit viral entry, the synthesis of negative-strand RNA in a virus, the budding of a virus, and the accumulation of reactive oxygen species (ROS) by porcine epidemic diarrhea virus (PEDV). The antiviral activity of CCM-CDs may also be ascribed to IFN-stimulating gene (ISG) proteins and proinflammatory cytokine production.

2. EXPERIMENTAL SECTION

2.1. Preparation of CCM-CDs. Curcumin (CCM; 0.30 g) and citric acid (0.60 g) were ground uniformly, sealed, and hydrothermally treated in a 25 mL Teflon-lined autoclave at 180 °C for 1 h. A total of 15 mL of ultrapure water was added to the brown mixture obtained from the reaction, followed by centrifugation to eliminate the large particles.[30] Finally, the as-prepared CDs (CCM-CDs) were dialyzed (the cutoff molecular weight of the dialysis membrane was 100 D) and then kept at low temperature. In the control experiment, 2.0 g of citric acid was poured into 8.0 mL of distilled water, and then 1.0 mL of ethylenediamine (EDA) was added to form a homogeneous solution. Then, the mixture was reacted at 200 °C for 3 h.[31] The obtained CDs (EDA-CDs) were also subjected to dialysis and purification and kept at low temperature.

2.2. Cytotoxicity Assay. Briefly, Vero cells were seeded, allowed to grow in a monolayer, and then incubated with CCM-CDs (15.6−250 μg/mL) for 24 and 48 h. Then a CCK-8 reagent was infected and cultured for 1 h.[32] The relative viability of the cells was counted based on the expressions: cell survival rate (%) = OD(sample)/OD(control) × 100%.

2.3. Entry Assay. Briefly, PEDV was exposed to various concentrations of CCM-CDs (37 °C, 1 h), added to 100% confluent Vero cells to allow the entry of virions and infection for another 1 h, and then coated with a medium. The cells continue to be cultured until the control group shows viral lysis plaques. The viral titers were measured via plaque assay.[33]

2.4. Penetration Assay. Vero cells were precooled (4 °C, 30 min), followed by infection with PEDV, to allow the attachment of virions to cells at 4 °C. After incubation for 2 h, the media containing different concentrations of CCM-CDs were supplemented, and the cells were maintained at 37 °C to start in penetration of the virus for 3 h. The remaining steps are consistent with the entry assay.[34]

2.5. Viral Negative-Strand RNA Replication. Vero cells were infected with PEDV at a multiplicity of infection (MOI) of 0.01 (1 h) and then cocultured with Dulbecco's modified Eagle medium (supplement 10 μg/mL trypsin) or CCM-CDs. At 5, 6, 7, and 8 hpi, the cell monolayer was harvested using the TRIzol reagent and the expression of PEDV negative-strand RNA was detected via real-time reverse transcription polymerase chain reaction (RT-PCR) according to the literature.[35]

2.6. Release Analysis. Vero cells were inoculated with PEDV at a MOI of 0.01 and incubated for the specified time. Then the supernatant was discarded, and the cells were then either not treated or treated with CCM-CDs for 15, 30, 45, and 60 min. Subsequently, medium supernatants and cell lysates, including progeny PEDV were harvested, respectively. The viral titer of samples was tested via plaque assay.

2.7. Determination of ROS Production. The ROS accumulation suppressed by CCM-CDs-exposed Vero cells was measured based on the previously reported method.[36] Briefly, PEDV infection of Vero cells was performed by preincubation with 10 μM dichlorofluorescein (DCF; 30 min, 37 °C) and then treatment with CCM-CDs for 12 h. The ROS level was visualized by a confocal laser scanning microscope.

2.8. Statistical Analysis. An independent t test or a one-way ANOVA test was used to analyze the experimental data. The values and error bars represent the mean values and standard deviations of three independent experiments, respectively. Statistical significances were expressed as $^{**}p < 0.01$ and $^{*}p < 0.05$.

3. RESULTS AND DISCUSSION

3.1. Preparation and Characterization of CCM-CDs. The optical properties of CCM-CDs was first characterized through UV−vis spectroscopy. In Figure 1a, the characteristic absorption peaks at about 282 and 225 nm should be attributed to n−π^* and π−π^* transitions, respectively. The fluorescence (FL) spectra showed that the maximum FL emission wavelength was 460 nm, suggesting a blue-light emission. Figure 1b shows a red shift of the emission wavelength of CCM-CDs from 460 to 501 nm in the excitation wavelength range from 310 to 400 nm. This phenomenon was called the excitation-dependent FL behavior, which was thought to be connected with the distribution of different sizes and surface states of CCM-CDs.[37] Besides, the FL spectra of CCM-CDs were detected after changing the time of pyrolysis. As displayed in Figure S1, the maximum FL emission wavelength of the CCM-CDs had an obvious red shift with an increase of the pyrolysis time, which was consistent with the conclusion of the quantum confinement effects.[38] In Figure 1c, the resulting CCM-CDs are uniform in size and spherical in shape. The lower right corner of Figure 1c shows that the average size of CCM-CDs is 1.5 ± 0.3 nm by high-resolution transmission electron microscopy (HRTEM) calculation. The Gaussian fitting curve revealed that the average diameters of CCM-CDs were 1.7 nm (Figure 1d) and the ζ potential of CCM-CDs was 15.6 ± 2.05 mV. Because the surface of the CCM-CDs was rich in hydroxyl groups, the solution is slightly acidic (pH = 6.8). The hydroxyl groups were hydrated with positively charged H_3O^+ in solution,[39] resulting in a certain degree of positive charge on the surface of the CCM-CDs.

The FL lifetime of the CCM-CDs was evaluated through time-correlated single photon counting (Figure S2). The average lifetime τ can be calculated by the equation $\tau = (B_1\tau_1^2 + B_2\tau_2^2)/(B_1\tau + B_2\tau_2)$.[40] Table S1 presents the fitting parameters of τ_1, τ_2, B_1, B_2, and τ, and the lifetime of the CCM-CDs was 8.81 ± 1.25 ns. Taking the quinine sulfate (quantum yield = 54%) as the standard, the quantum yield of the CCM-CDs was calculated to be 3.6% based on the previously reported procedure.[41,42]

In Figure S3a, both CCM and CCM-CDs show different functional groups except for the phenolic hydroxyl group. The absorption band at 3200−3400 cm^{-1} was due to the stretching

DOI: 10.1021/acsanm.8b00779
ACS Appl. Nano Mater. 2018, 1, 5451−5459

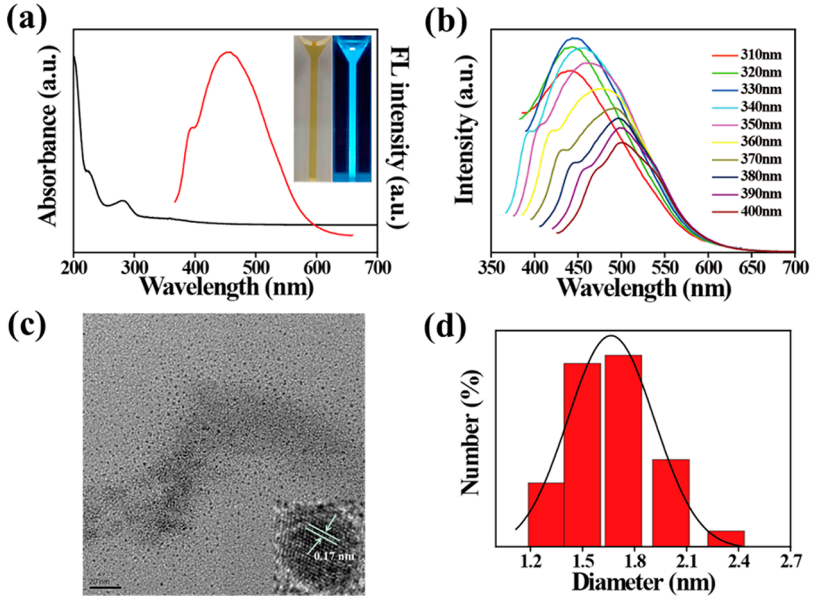

Figure 1. (a) UV−vis absorption and FL emission spectra of CCM-CDs in aqueous solution. (b) Excitation-dependent FL for CCM-CDs. (c) TEM and HRTEM images. Scale bar: 20 nm. (d) Size distribution of CCM-CDs.

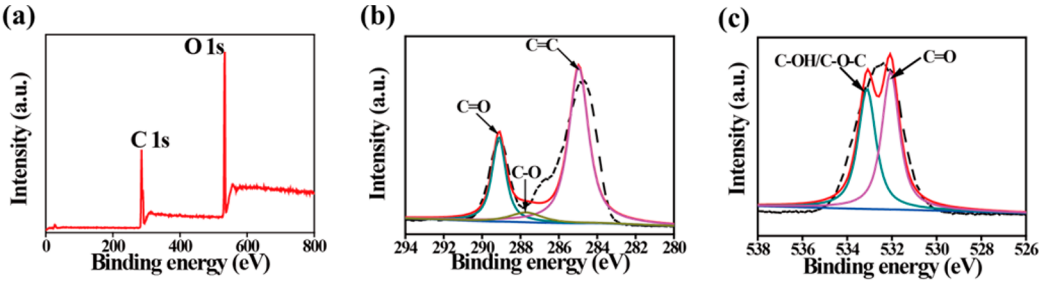

Figure 2. XPS survey spectra of CCM-CDs derived from CCM: (a) overall spectrum; (b) C 1s and (c) O 1s high-resolution survey spectra of the CCM-CDs.

vibration of the phenolic hydroxyl groups, which appeared in either CCM or CCM-CDs. The phenolic hydroxyl groups in CCM may play viral roles in its antioxidant, anti-inflammatory, and radical scavenging activities, implying potential vital roles of the phenolic hydroxyl groups in the antiviral activity of CCM-CDs. Besides, the band observed at 1622 cm^{-1} in CCM is due to the C═O vibration, which shifted to 1650 cm^{-1} in CCM-CDs. The peaks at 1217 and 1019 cm^{-1} for CCM explicitly demonstrated the existence of C−O−C and C−O, which disappeared in CCM-CDs. In Figure S3b, the X-ray diffraction pattern demonstrates the crystalline nature of the sample. Because of their nanoscale size, the diffraction peaks of the CCM-CDs distinctly broadened, suggesting the existence of CDs. The characteristic bands in the Raman spectra of CCM-CDs were located at around 1345 and 1595 cm^{-1}, corresponding to the D and G bands, respectively (Figure S3c).[43,44]

The overall X-ray photoelectron spectroscopy (XPS) analysis of the CCM-CDs showed that there were two bands at 284.1 and 533.1 eV, corresponding to C 1s and O 1s (Figure 2a). The C 1s peaks at 284.6 and 288.8 eV (Figure 2b) attributed to the C−C and C═O functions, indicating that the synthetic CCM-CDs surface was rich in hydrophilic groups.[7] The contributions at 531.8 and 533.0 eV of O 1s were due to the C═O and C−OH/C−O−C functions (Figure 2c).[45] The surface composition of the CCM-CDs, as determined by XPS, was inaccordance with the corresponding Fourier transform infrared (FTIR) conclusion. These results indicated that the remaining CCM and citrate were not carbonized and remained on the surface of the CDs as protective groups.

3.2. Toxicity of CCM-CDs on Cells. The in vitro cytotoxicity of CCM-CDs against Vero and PK-15 cells was evaluated via CCK-8 assay (Figures 3 and S4). Presented in

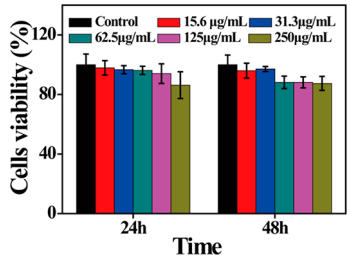

Figure 3. Effects of different concentrations of CCM-CDs on the Vero cell viability detected by CCK-8 assay.

Figure 3 are the survival rates of Vero cells exposed to various concentrations of CCM-CDs for different incubation times (24 and 48 h). As expected, Vero cells were coincubated with CCM-CDs concentration ranges from 15.6 to 125 μg/mL in vitro and the cell viability was observed to exceed 90% after 24 and 48 h, confirming the low cytotoxicity of the as-prepared CCM-CDs. To test whether dimethyl sulfoxide (DMSO) had

DOI: 10.1021/acsanm.8b00779
ACS Appl. Nano Mater. 2018, 1, 5451−5459

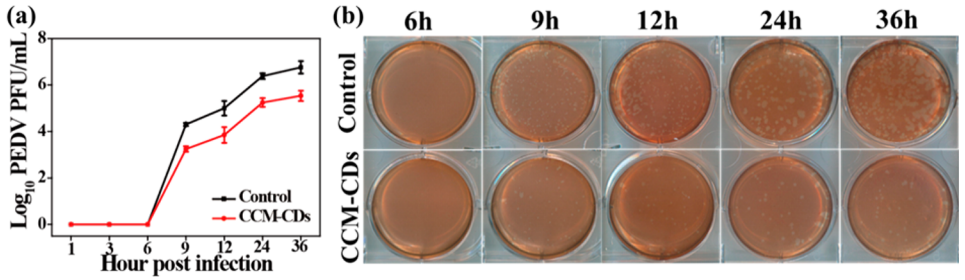

Figure 4. (a) One-step growth curves of a virus in the absence and presence of CCM-CDs. (b) Virus titers detected in the presence and absence of CCM-CDs and photographs taken 2−3 days postinfection.

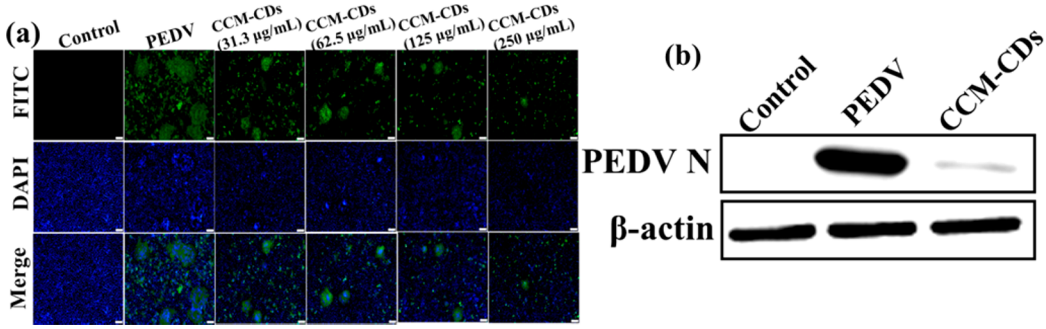

Figure 5. Effect of the CCM-CDs on PEDV: (a) Effect of different concentrations of CCM-CDs on PEDV-infected Vero cells by indirect immunofluorescence assay. Scale bar: 100 μm. (b) Expression level of PEDV nitrogen protein in the presence of 125 μg/mL CCM-CDs at 12 hpi by Western blot analysis.

an effect on the stability of CCM-CDs at low concentrations, the particle size of CCM-CDs in DMSO was measured. The average hydrodynamic size was 1.6 nm (Figure S5). This was close to the size measured when the solvent was water, indicating that the effect of DMSO on CCM-CDs could be ignored. Thus, 125 μg/mL CCM-CDs was used for the following antiviral experiments.

3.3. Antiviral Activity of CCM-CDs against PEDV Infection. The inhibitory effect of the CCM-CDs was investigated through one-step growth curve assay to evaluate the infectivity of PEDV. Specifically, the replication of PEDV in Vero cells was determined with the treatment and nontreatment of 125 μg/mL CCM-CDs, followed by the quantification of viral titers. As displayed in Figure 4a, compared with the control groups, the virus titers of the experimental groups are obviously reduced, demonstrating the efficient inhibitory effect of the CCM-CDs on PEDV infection. Meanwhile, it can be visually observed that the plaque numbers are distinctly reduced upon exposure with CCM-CDs (Figure 4b). The reduction of the plaque numbers and decrease of the virus titers indicate that CCM-CDs can effectively inhibit virus replication.

The protective effects of CCM-CDs were detected by fluorescent inverted microscopy. In Figure S6a, no cytopathic effect (CPE) is noticed in the negative control group. Cells treated with PEDV show lysis and detachment from the cell monolayer at 12 h postinfection (hpi; Figure S6b). However, the CPE gradually diminishes upon treatment with different concentrations of CCM-CDs (Figure S6c,d). These results suggested that CCM-CDs interfered with the infectivity of PEDV.

To study the inhibitory effect of CCM-CDs, the expression of PEDV nitrogen proteins in Vero cells was detected. In Figure 5a, the green FL signals of the experimental groups are dramatically reduced, which is directly reflected in the decrease of the expression level of PEDV nitrogen protein. These results were confirmed by Western blot analysis (Figure 5b). To test whether the quenching effect of CDs will influence the FL, the FL image was observed by using a confocal laser scanning microscope. A weak blue FL could be observed, indicating that CCM-CDs can be taken by Vero cells (Figure S7). However, the FL of CCM-CDs can be neglected in comparison with that of fluorescein isothiocyanate and 4′,6-diamidino-2-phenylindole. These results excluded the probability that the aforementioned reduction of viral titers resulted from the cellular toxicity of the CCM-CDs.

The antiviral activity of CCM-CDs was also compared to that of EDA-CDs because EDA is a common surface passivation reagent for the preparation of high-yield CDs.[31] The optical properties and surface functional groups of the EDA-CDs are displayed in Figure S8. In Figure 6a, it is found to be almost impossible for EDA-CDs to suppress the virus infection at all tested concentrations. In Figure 6b,c, the virus titer values and plaque numbers reveal that CCM-CDs has a antiviral effect superior to that of EDA-CDs. The CCM-CDs show a higher ζ potential (+15.6 mV) than EDA-CDs (−5.1 mV). Moreover, the effect of a positively charged CD (33 mV) on the PEDV nitrogen protein was also analyzed by Western blot. From Figure S9, it can be seen that the positively charged CDs show a decrease in the PEDV nitrogen protein expression over that of the control groups. We speculate that the surface charge of the CCM-CDs plays a small part in their antiviral efficacy. The positively charged CCM-CDs on the surface undergo strong electrostatic interactions with PEDV or cell membranes, thereby competing to bind the virus to cells.

3.4. Mechanism of Viral Inhibition. The proposed antiviral mechanisms of CCM-CDs cover direct action on the viral entry, penetration, replication, and budding.[46] Thus, a set of experiments were carried out to identify which stage(s) of the viral life cycle were suppressed by CCM-CDs.

DOI: 10.1021/acsanm.8b00779
ACS Appl. Nano Mater. 2018, 1, 5451−5459

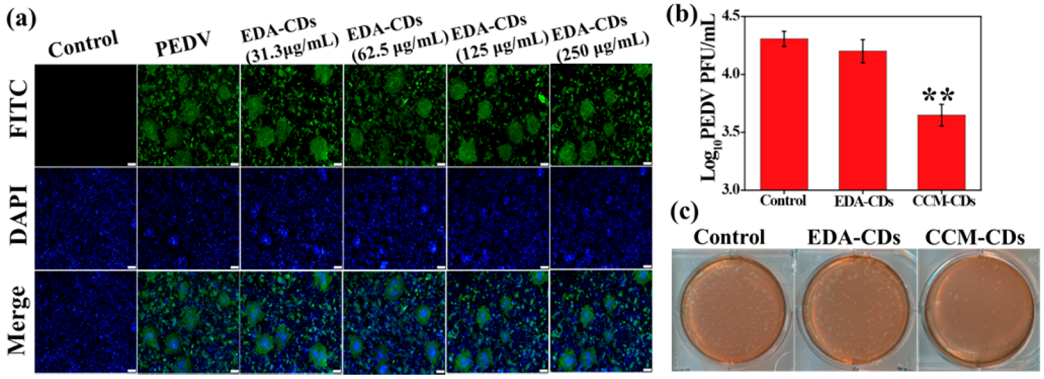

Figure 6. Effects of the EDA-CDs on PEDV: (a) Effect of different concentrations of EDA-CDs on PEDV-infected Vero cells by indirect immunofluorescence assay. Scale bar: 100 μm. (b) Titers of PEDV when exposed or unexposed to 125 μg/mL EDA-CDs or CCM-CDs. All error bars were determined according to three replicate experiments. (c) Virus titers calculated in the presence and absence of EDA-CDs or CCM-CDs. The pictures were taken at 12 hpi.

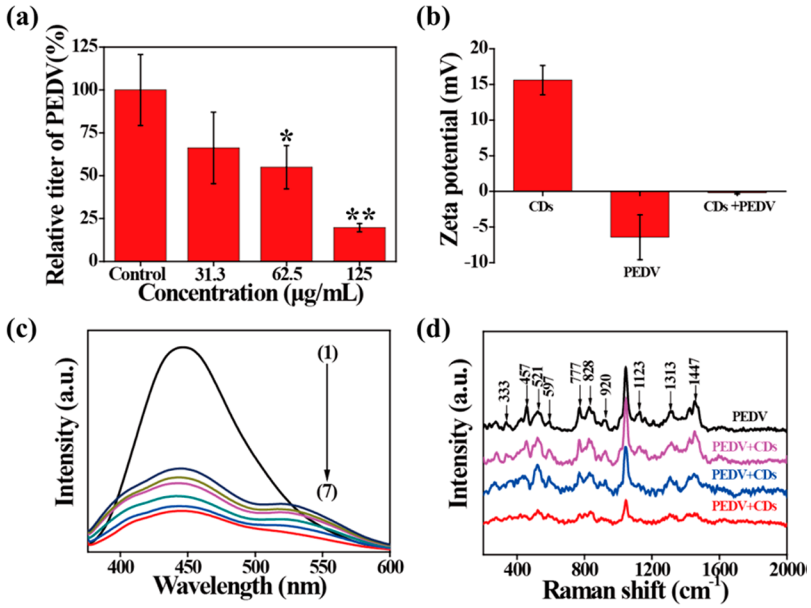

Figure 7. (a) Dose relationship between the viral entry inhibitory efficiency and amount of CCM-CDs added. (b) ζ potentials of the CCM-CDs, PEDV, and CCM-CDs pretreated with PEDV, respectively. (c) FL spectra of CCM-CDs. CCM-CDs (125 μg/mL) were exposed to PEDV (1−7: 0, 1×10^5, 2×10^5, 3×10^5, 4×10^5, 5×10^5, and 6×10^5 PFU/mL). (d) Raman spectral analysis of PEDV and CCM-CDs-treated PEDV. The black line is PEDV (10^5 PFU/mL), the pink line represents PEDV (10^5 PFU/mL) pretreated with 31.3 μg/mL CCM-CDs, the blue line represents PEDV (10^5 PFU/mL) pretreated with 62.5 μg/mL CCM-CDs, and the red line indicates PEDV (10^5 PFU/mL) pretreated with 125 μg/mL CCM-CDs, respectively.

The influence of CCM-CDs on the virus entry was evaluated by using plaque reduction analysis. PEDV samples were first treated with different concentrations of CCM-CDs and then inoculated into the cells (37 °C, 1 h). In Figure 7a, CCM-CDs show a strong concentration-dependent inhibitory effect on PEDV, suggesting that they block PEDV infection at the early stages of viral entry. The inhibition efficiency of CCM-CDs (125 μg/mL) on virus entry was over 50%. Furthermore, the ζ potentials of CCM-CDs, PEDV, and CCM-CDs pretreated with PEDV were measured, and they were +15.6, −6.42, and −0.18 mV, respectively (Figure 7b), implying that the positively charged CCM-CDs may cause virus aggregation through electrostatic interaction, resulting in reduced viral infectivity. These results were verified through FL and Raman spectral analysis. Figure 7c shows that the FL intensity and maximum emission of CCM-CDs decreased gradually and exhibited an apparent red shift along with and increase of the PEDV concentration, indicating the occurrence of interaction between CCM-CDs and PEDV.[47] To demonstrate the interaction between CCM-CDs and PEDV, Raman displacement tests were carried out for PEDV when it was exposed or not exposed to different concentrations of CCM-CDs. From Figure 7d, it can be seen that, with increasing amount of CCM-CDs, the Raman spectra exhibit the most obvious differences in the shifts of 333, 457, 521, 597, 777, 828, 920, 1123, 1313, and 1447 cm^{-1}. The peaks at 521 and 777 cm^{-1} are attributed to S−S disulfide stretch in proteins and cytosine/uracil ring breathing, respectively.[48] The peak at 828 cm^{-1} is assigned to the out-of-plane ring breathing tyrosine. The bands at 920, 1123, 1313, and 1447 cm^{-1} correspond to the C−C stretch of the proline ring, C−C stretching mode of lipids/protein, CH_3CH_2 twisting mode of collagen/lipids, and CH_2 bending mode of proteins and lipids.[49,50] These observations suggest that the addition of CCM-CDs changed the structure of the protein.

DOI: 10.1021/acsanm.8b00779
ACS Appl. Nano Mater. 2018, 1, 5451−5459

In order to test whether CCM-CDs can inhibit viral penetration, different concentrations of CCM-CDs were injected after PEDV was attached to the cell surface (4 °C, 2 h), and then penetration was started by transferring the temperature to 37 °C. In Figure 8a, no noticeable difference is observed from

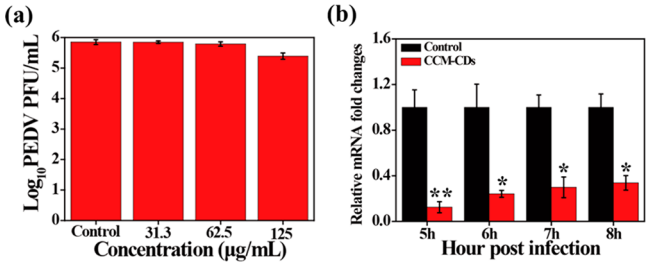

Figure 8. (a) Dose relationship between the viral entry inhibitory efficiency and amount of CCM-CDs used. (b) Relative synthesis of PEDV negative-strand RNA measured after infection for various times.

viral titers after treatment or no treatment with CCM-CDs, indicating that the CCM-CDs did not inhibit viral penetration. It is well documented that the synthesis of PEDV negative-strand RNA begins soon after penetration into the infected cells. The inhibitory activity of CCM-CDs on the negative-strand RNA synthesis was evaluated. The negative-strand RNA level of PEDV showed a remarkable downregulation in CCM-CDs-treated cells compared to the untreated control at different hours postinfection, suggesting that CCM-CDs can effectively inhibit PEDV at the replication step (Figure 8b).

To probe the influence of CCM-CDs on virion budding, viral titers in the intracellular and supernatant after various times of CCM-CDs treatment were quantified. In Figure 9a,

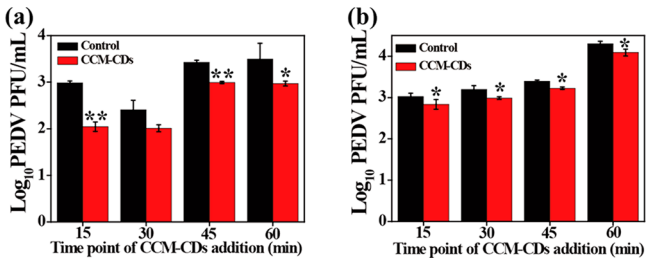

Figure 9. Titers of PEDV quantified after treatment with CCM-CDs at different time points: viral titers in (a) intracellular and (b) supernatant.

significant differences were detected in PEDV intracellular titers between the CCM-CDs-treated and control groups, whereas the virus titer in the supernatant treated with CCM-CDs was only slightly less than that in the control group, indicating that CCM-CDs could inhibit viral budding (Figure 9b).

3.5. CCM-CDs Activation of Antiviral Innate Immunity. Innate immune response offers the first line of defense against the invasion of pathogens and limits their spread.[51,52] Incoming viruses can activate nuclear factor-κB (NF-κB) and/or IFN regulatory factors (IRFs) to induce the expression of hundreds of antiviral cytokines, including IFNs and proinflammatory cytokines. An antiviral IFNs signal via the JAK/STAT pathway drives the synthesis of a great nmuber of ISGs or through direct stimulation in an IFN-independent pathway collaboratively stops different stages of viral replication during the viral replication cycle.[53] To investigate whether CCM-CDs can trigger a host innate immune response, we examined the influence of CCM-CDs on the expressions of ISGs and proinflammatory cytokines in vitro by measuring their mRNA levels using RT-PCR (Figures S10 and S11). After CCM-CDs treatment, an obviously upregulated expression can be observed in IFN-inducible protein 10 (IP-10; Figure S10a), IFN-stimulated gene 54 (ISG-54; Figure S10b), MxA (Figure S10c), and IFN-stimulated gene 20 (ISG-20; Figure S10f). The mRNA expression levels of interleukin 8 (IL-8; Figure S10d) and interleukin 6 (IL-6; Figure S10e) were also 5.8- and 3.0-fold more in cells treated with CCM-CDs than in the untreated controls. It was found that TRIM32 can be used as an antiviral factor mainly by activating the IFN immune response and promoting the expression of IL-8 and IL-6.[54] This was consistent with our conclusion.

The cooperativity of the transcription factors IRF3 and NF-κB is necessary for the induction of ISGs and proinflammatory cytokines. To examine whether CCM-CDs induced expression of IRF-3 and NF-κB, Vero cells were first exposed or not exposed with CCM-CDs, and then IRF3-Luc, NF-κB-Luc luciferase reporter plasmids, and internal control plasmid pRL-TK were cotransfected. As demonstrated in Figure 10a,b, the

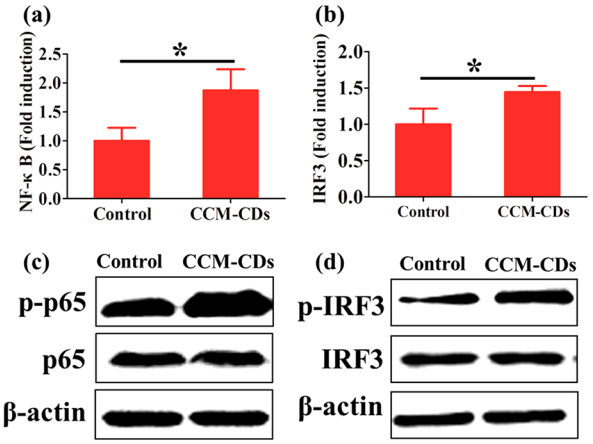

Figure 10. CCM-CDs upregulation of expression of IRF3 and NF-κB promoters. Cells were cotransfected with NF-κB-Luc (a) and IRF3-Luc (b), together with the pRL-TK plasmid. Upon exposure with CCM-CDs for 12 h, the luciferase test was carried out. CCM-CDs treatment stimulated phosphorylation of IRF3 and p65 (c and d). Cells were treated with CCM-CDs for 12 h, and then cells were harvested and detected by Western blot assays with specific antibodies.

CCM-CDs can upregulate the IRF3 and NF-κB promoter activity. Moreover, the production of phosphorylated IRF3 (p-IRF3) and p65 (p-p65) proteins in the CCM-CDs treatment group is dramatically higher than that in the control group (Figure 10c,d). Phosphorylation of IRF3 and NF-κB subunit p65 was considered to be the sign of IRF3 and NF-κB. Collectively, all of these data revealed that innate immune response might be triggered in vitro by the CCM-CDs treatment.

3.6. Inhibition on ROS Generation by CCM-CDs. The infection of certain viruses occurs simultaneously with the overexpression of ROS, leading to DNA damage by regulating apoptotic signaling pathways. In order to probe whether CCM-CDs can suppress ROS generation, a 2′,7′-dichlorodihydrofluorescein diacetate test was performed. The stronger fluorescent intensity of DCF was observed in PEDV-infected cells compared to the control group (Figure S12a,b). However, after treatment with CCM-CDs, the FL intensity turned weak (Figure S12c).

DOI: 10.1021/acsanm.8b00779
ACS Appl. Nano Mater. 2018, 1, 5451−5459

Because most CCM was carbonized at high temperatures, the prepared CCM-CDs was centrifuged and dialyzed to remove unreacted small molecules. The presence of free CCM was excluded, which indicated that CCM-CDs could inhibit ROS generation induced by PEDV infection.

4. CONCLUSION

In conclusion, the fluorescent CCM-CDs were obtained by a simple one-step method of the pyrolysis of CCM, and its detailed characterization was performed. The characterization results showed that the CCM-CDs had an ultrasmall size (diameter ca. 1.5 nm), rich hydrophilic groups, and a positive potential (+15.6 mV).

This is the first report showing that CCM-CDs obtained by the pyrolysis of herbs have prominent antiviral activity against PEDV infection. Compared with the common CDs synthesized by the pyrolysis of EDA, cationic CCM-CDs possess better antiviral properties. The underlying mechanism analysis indicates that CCM-CDs exposure can inhibit viral entry by changing the structure of the viral surface protein and prevent the synthesis and budding of negative-strand RNA in the virus. It has also been demonstrated that CCM-CDs could obviously suppress the accumulation of ROS caused by PEDV. Furthermore, CCM-CDs treatment can suppress virus reproduction by activating the production of ISGs and proinflammatory cytokines of Vero cells.

Our results provide a novel clue to improve the antiviral activity of herbs. The integrated data indicate that CCM-CDs can be potentially applied against not only PEDV but also other viruses. However, further evaluation needs to be performed on the prophylactic and therapeutic effects of CCM-CDs using an appropriate animal model.

■ ASSOCIATED CONTENT

Supporting Information

The Supporting Information is available free of charge on the ACS Publications website at DOI: 10.1021/acsanm.8b00779.

Experimental section, synthesis routes of CCM-CDs (Scheme S1), fluorescent spectra (Figure S1), FL decay curves (Figure S2), fitting parameters of CCM-CDs (Table S1), FTIR spectra, Raman specta and XRD patterns of CCM-CDs (Figure S3), CPEs of Vero cells (Figures S4 and S6), size distribution (Figure S5), FL microscopy images (Figure S7), characterization of EDA-CDs (Figure S8), Western blot (Figure S9), real-time RT-PCR assay (Figures S10 and S11), indirect immunofluorescence assay (Figure S12), and primers sequence (Table S2) (PDF)

■ AUTHOR INFORMATION

Corresponding Authors

*E-mail: hyhan@mail.hzau.edu.cn.
*E-mail: vet@mail.hzau.edu.cn.

ORCID

Shaobo Xiao: 0000-0003-0023-9188
Heyou Han: 0000-0001-9406-0722

Author Contributions

⊥These authors jointly supervised this work.

Notes

The authors declare no competing financial interest.

■ ACKNOWLEDGMENTS

This research was supported by the National Key R&D Program (Grant 2016YFD0500700), the National Natural Science Foundation of China (Grants 21375043, 21778020, 31672569, and 31402239), and the Sci-tech Innovation Foundation of Huazhong Agriculture University (Grant 2662017PY042).

■ REFERENCES

(1) Lv, Y. L.; Gong, L. L.; Wang, Z. H.; Han, F. F.; Liu, H.; Lu, X. C.; Liu, L. H. Curcumin Inhibits Human Cytomegalovirus by Downregulating Heat Shock Protein 90. *Mol. Med. Rep.* **2015**, *12*, 4789−4793.

(2) Teymouri, M.; Pirro, M.; Johnston, T. P.; Sahebkar, A. Curcumin as a Multifaceted Compound against Human Papilloma Virus Infection and Cervical Cancers: A Review of Chemistry, Cellular, Molecular, and Preclinical Features. *BioFactors* **2017**, *43*, 331−346.

(3) Zheng, M.; Liu, S.; Guan, X. G.; Xie, Z. G. One-Step Synthesis of Nanoscale Zeolitic Imidazolate Frameworks with High Curcumin Loading for Treatment of Cervical Cancer. *ACS Appl. Mater. Interfaces* **2015**, *7*, 22181−22187.

(4) Mouler Rechtman, M.; Har Noy, O.; Bar Yishay, I.; Fishman, S.; Adamovich, Y.; Shaul, Y.; Halpern, Z.; Shlomai, A. Curcumin Inhibits Hepatitis B Virus via Down-Regulation of the Metabolic Coactivator PGC-1α. *FEBS Lett.* **2010**, *584*, 2485−2490.

(5) Ali, A.; Banerjea, A. C. Curcumin Inhibits HIV-1 by Promoting Tat Protein Degradation. *Sci. Rep.* **2016**, *6*, 27539−27548.

(6) Narayanan, A.; Kehn Hall, K.; Senina, S.; Lundberg, L.; Van Duyne, R.; Guendel, I.; Das, R.; Baer, A.; Bethel, L.; Turell, M.; Hartman, A. L.; Das, B.; Bailey, C.; Kashanchi, F. Curcumin Inhibits Rift Valley Fever Virus Replication in Human Cells. *J. Biol. Chem.* **2012**, *287*, 33198−33214.

(7) Yang, X. X.; Li, C. M.; Huang, C. Z. Curcumin Modified Silver Nanoparticles for Highly Efficient Inhibition of Respiratory Syncytial Virus Infection. *Nanoscale* **2016**, *8*, 3040−3048.

(8) Yang, X. X.; Li, C. M.; Li, Y. F.; Wang, J.; Huang, C. Z. Synergistic Antiviral Effect of Curcumin Functionalized Graphene Oxide against Respiratory Syncytial Virus Infection. *Nanoscale* **2017**, *9*, 16086−16092.

(9) Lembo, D.; Cavalli, R. Nanoparticulate Delivery Systems for Antiviral Drugs. *Antivir. Chem. Chemoth.* **2010**, *21*, 53−70.

(10) Szunerits, S.; Barras, A.; Khanal, M.; Pagneux, Q.; Boukherroub, R. Nanostructures for the Inhibition of Viral Infections. *Molecules* **2015**, *20*, 14051−14081.

(11) Yadavalli, T.; Shukla, D. Role of Metal and Metal Oxide Nanoparticles as Diagnostic and Therapeutic Tools for Highly Prevalent Viral Infections. *Nanomedicine* **2017**, *13*, 219−230.

(12) Singh, L.; Kruger, H. G.; Maguire, G. E. M.; Govender, T.; Parboosing, R. The Role of Nanotechnology in the Treatment of Viral Infections. *Ther. Adv. Infect. Dis.* **2017**, *4*, 105−131.

(13) Draz, M. S.; Wang, Y. J.; Chen, F. F.; Xu, Y. H.; Shafiee, H. Electrically Oscillating Plasmonic Nanoparticles for Enhanced DNA Vaccination against Hepatitis C Virus. *Adv. Funct. Mater.* **2017**, *27*, 1604139−1604149.

(14) Vonnemann, J.; Sieben, C.; Wolff, C.; Ludwig, K.; Bottcher, C.; Herrmann, A.; Haag, R. Virus Inhibition Induced by Polyvalent Nanoparticles of Different Sizes. *Nanoscale* **2014**, *6*, 2353−2360.

(15) Li, L.; Fu, F.; Xue, M.; Chen, W.; Liu, J.; Shi, H.; Chen, J.; Bu, Z.; Feng, L.; Liu, P. IFN-Lambda Preferably Inhibits PEDV Infection of Porcine Intestinal Epithelial Cells Compared with IFN-Alpha. *Antiviral Res.* **2017**, *140*, 76−82.

(16) Bhatia, S.; Lauster, D.; Bardua, M.; Ludwig, K.; Angioletti-Uberti, S.; Popp, N.; Hoffmann, U.; Paulus, F.; Budt, M.; Stadtmuller, M.; Wolff, T.; Hamann, A.; Bottcher, C.; Herrmann, A.; Haag, R. Linear Polysialoside Outperforms Dendritic Analogs for Inhibition of Influenza Virus Infection in Vitro and in Vivo. *Biomaterials* **2017**, *138*, 22−34.

DOI: 10.1021/acsanm.8b00779
ACS Appl. Nano Mater. 2018, 1, 5451−5459

(17) Ziem, B.; Azab, W.; Gholami, M. F.; Rabe, J. P.; Osterrieder, N.; Haag, R. Size-Dependent Inhibition of Herpesvirus Cellular Entry by Polyvalent Nanoarchitectures. *Nanoscale* **2017**, *9*, 3774−3783.
(18) Ziem, B.; Rahn, J.; Donskyi, I.; Silberreis, K.; Cuellar, L.; Dernedde, J.; Keil, G.; Mettenleiter, T. C.; Haag, R. Polyvalent 2D Entry Inhibitors for Pseudorabies and African Swine Fever Virus. *Macromol. Biosci.* **2017**, *17*, 1600499.
(19) Kwon, S. J.; Na, D. H.; Kwak, J. H.; Douaisi, M.; Zhang, F.; Park, E. J.; Park, J. H.; Youn, H.; Song, C. S.; Kane, R. S.; Dordick, J. S.; Lee, K. B.; Linhardt, R. J. Nanostructured Glycan Architecture is Important in the Inhibition of Influenza A Virus Infection. *Nat. Nanotechnol.* **2016**, *12*, 48−54.
(20) Castro-Mayorga, J. L.; Randazzo, W.; Fabra, M. J.; Lagaron, J. M.; Aznar, R.; Sánchez, G. Antiviral Properties of Silver Nanoparticles against Norovirus Surrogates and Their Efficacy in Coated Polyhydroxyalkanoates Systems. *LWT Food Sci. Technol.* **2017**, *79*, 503−510.
(21) Lv, X.; Wang, P.; Bai, R.; Cong, Y.; Suo, S.; Ren, X.; Chen, C. Inhibitory Effect of Silver Nanomaterials on Transmissible Virus-Induced Host Cell Infections. *Biomaterials* **2014**, *35*, 4195−4203.
(22) Akbarzadeh, A.; Kafshdooz, L.; Razban, Z.; Dastranj Tbrizi, A.; Rasoulpour, S.; Khalilov, R.; Kavetskyy, T.; Saghfi, S.; Nasibova, A. N.; Kaamyabi, S.; Kafshdooz, T. An Overview Application of Silver Nanoparticles in Inhibition of Herpes Simplex Virus. *Artif. Cells, Nanomed., Biotechnol.* **2018**, *46*, 263−267.
(23) Nagy, A.; Steinbrück, A.; Gao, J.; Doggett, N.; Hollingsworth, J. A.; Iyer, R. Comprehensive Analysis of the Effects of CdSe Quantum Dot Size, Surface Charge, and Functionalization on Primary Human Lung Cells. *ACS Nano* **2012**, *6*, 4748−4762.
(24) Liu, X.; Huang, N.; Li, H.; Jin, Q.; Ji, J. Surface and Size Effects on Cell Interaction of Gold Nanoparticles with both Phagocytic and Nonphagocytic Cells. *Langmuir* **2013**, *29*, 9138−9148.
(25) Deokar, A. R.; Nagvenkar, A. P.; Kalt, I.; Shani, L.; Yeshurun, Y.; Gedanken, A.; Sarid, R. Graphene-Based "Hot Plate" for the Capture and Destruction of the Herpes Simplex Virus Type 1. *Bioconjugate Chem.* **2017**, *28*, 1115−1122.
(26) Barras, A.; Pagneux, Q.; Sane, F.; Wang, Q.; Boukherroub, R.; Hober, D.; Szunerits, S. High Efficiency of Functional Carbon Nanodots as Entry Inhibitors of Herpes Simplex Virus Type 1. *ACS Appl. Mater. Interfaces* **2016**, *8*, 9004−9013.
(27) Liu, Y.; Yan, B.; Winkler, D. A.; Fu, J.; Zhang, A. Competitive Inhibition Mechanism of Acetylcholinesterase without Catalytic Active Site Interaction: Study on Functionalized C60 Nanoparticles via in Vitro and in Silico Assays. *ACS Appl. Mater. Interfaces* **2017**, *9*, 18626−18638.
(28) Sametband, M.; Kalt, I.; Gedanken, A.; Sarid, R. Herpes Simplex Virus Type-1 Attachment Inhibition by Functionalized Graphene Oxide. *ACS Appl. Mater. Interfaces* **2014**, *6*, 1228−1235.
(29) Du, T.; Liang, J. G.; Dong, N.; Liu, L.; Fang, L. R.; Xiao, S. B.; Han, H. Y. Carbon Dots as Inhibitors of Virus by Activation of Type I Interferon Response. *Carbon* **2016**, *110*, 278−285.
(30) Zhang, H.; Chen, Y.; Liang, M.; Xu, L.; Qi, S.; Chen, H.; Chen, X. Solid-Phase Synthesis of Highly Fluorescent Nitrogen-Doped Carbon Dots for Sensitive and Selective Probing Ferric Ions in Living Cells. *Anal. Chem.* **2014**, *86*, 9846−9852.
(31) Li, F.; Liu, C.; Yang, J.; Wang, Z.; Liu, W.; Tian, F. Mg/N Double Doping Strategy to Fabricate Extremely High Luminescent Carbon Dots for Bioimaging. *RSC Adv.* **2014**, *4*, 3201−3205.
(32) Yang, S. T.; Wang, X.; Wang, H.; Lu, F.; Luo, P. G.; Cao, L.; Meziani, M. J.; Liu, J. H.; Liu, Y.; Chen, M.; Huang, Y.; Sun, Y. P. Carbon Dots as Nontoxic and High-Performance Fluorescence Imaging Agents. *J. Phys. Chem. C* **2009**, *113*, 18110−18114.
(33) Alvarez, A. L.; Melon, S.; Dalton, K. P.; Nicieza, I.; Roque, A.; Suarez, B.; Parra, F. Apple Pomace, a by-Product from the Asturian Cider Industry, Inhibits Herpes Simplex Virus Types 1 and 2 in Vitro Replication: Study of its Mechanisms of Action. *J. Med. Food* **2012**, *15*, 581−587.
(34) Gescher, K.; Hensel, A.; Hafezi, W.; Derksen, A.; Kühn, J. Oligomeric Proanthocyanidins from Rumex Acetosa L. Inhibit the Attachment of Herpes Simplex Virus Type-1. *Antiviral Res.* **2011**, *89*, 9−18.
(35) Duan, E.; Wang, D.; Fang, L.; Ma, J.; Luo, J.; Chen, H.; Li, K.; Xiao, S. Suppression of Porcine Reproductive and Respiratory Syndrome Virus Proliferation by Glycyrrhizin. *Antiviral Res.* **2015**, *120*, 122−125.
(36) Li, Y. H.; Lin, Z. F.; Zhao, M. Q.; Xu, T. T.; Wang, C. B.; Hua, L.; Wang, H. Z.; Xia, H. M.; Zhu, B. Silver Nanoparticle Based Codelivery of Oseltamivir to Inhibit the Activity of the H1N1 Influenza Virus through ROS-Mediated Signaling Pathways. *ACS Appl. Mater. Interfaces* **2016**, *8*, 24385−24393.
(37) Gao, T.; Wang, X.; Yang, L. Y.; He, H.; Ba, X. X.; Zhao, J.; Jiang, F. L.; Liu, Y. Red, Yellow, and Blue Luminescence by Graphene Quantum Dots: Syntheses, Mechanism, and Cellular Imaging. *ACS Appl. Mater. Interfaces* **2017**, *9*, 24846−24856.
(38) Bera, D.; Qian, L.; Tseng, T. K.; Holloway, P. H. Quantum Dots and Their Multimodal Applications: A Review. *Materials* **2010**, *3*, 2260−2345.
(39) Leng, C.; Hung, H.-C.; Sun, S.; Wang, D.; Li, Y.; Jiang, S.; Chen, Z. Probing the Surface Hydration of Nonfouling Zwitterionic and PEG Materials in Contact with Proteins. *ACS Appl. Mater. Interfaces* **2015**, *7*, 16881−16888.
(40) Fu, Y. Y.; Guan, E. L.; Liang, J. G.; Ren, G. L.; Chen, L. Probing the Effect of Ag_2S Quantum Dots on Human Serum Albumin Using Spectral Techniques. *J. Nanomater.* **2017**, *2017*, 1−7.
(41) Fan, R. J.; Sun, Q.; Zhang, L.; Zhang, Y.; Lu, A. H. Photoluminescent Carbon Dots Directly Derived from Polyethylene Glycol and their Application for Cellular Imaging. *Carbon* **2014**, *71*, 87−93.
(42) Xiao, D.; Pan, R.; Li, S.; He, J.; Qi, M.; Kong, S.; Gu, Y.; Lin, R.; He, H. Porous Carbon Quantum Dots: One Step Green Synthesis Vial-Cysteine and Applications in Metal Ion Detection. *RSC Adv.* **2015**, *5*, 2039−2046.
(43) Bao, L.; Zhang, Z. L.; Tian, Z. Q.; Zhang, L.; Liu, C.; Lin, Y.; Qi, B.; Pang, D. W. Electrochemical Tuning of Luminescent Carbon Nanodots: from Preparation to Luminescence Mechanism. *Adv. Mater.* **2011**, *23*, 5801−5806.
(44) Fan, Z. J.; Kai, W.; Yan, J.; Wei, T.; Zhi, L. J.; Feng, J.; Ren, Y. M.; Song, L. P.; Wei, F. Facile Synthesis of Graphene Nanosheets via Fe Reduction of Exfoliated Graphite Oxide. *ACS Nano* **2011**, *5*, 191−198.
(45) Zhang, H. J.; Chen, Y. L.; Liang, M. J.; Xu, L. F.; Qi, S. D.; Chen, H. L.; Chen, X. G. Solid-Phase Synthesis of Highly Fluorescent Nitrogen-Doped Carbon Dots for Sensitive and Selective Probing Ferric Ions in Living Cells. *Anal. Chem.* **2014**, *86*, 9846−9852.
(46) Li, C. M.; Zheng, L. L.; Yang, X. X.; Wan, X. Y.; Wu, W. B.; Zhen, S. J.; Li, Y. F.; Luo, L. F.; Huang, C. Z. DNA-AuNP Networks on Cell Membranes as a Protective Barrier to Inhibit Viral Attachment, Entry and Budding. *Biomaterials* **2016**, *77*, 216−226.
(47) Lin, N.; Hu, F.; Sun, Y.; Wu, C.; Xu, H.; Liu, X. Y. Construction of White-Light-Emitting Silk Protein Hybrid Films by Molecular Recognized Assembly among Hierarchical Structures. *Adv. Funct. Mater.* **2014**, *24*, 5284−5290.
(48) Chan, J. W.; Taylor, D. S.; Zwerdling, T.; Lane, S. M.; Ihara, K.; Huser, T. Micro-Raman Spectroscopy Detects Individual Neoplastic and Normal Hematopoietic Cells. *Biophys. J.* **2006**, *90*, 648−656.
(49) Stone, N.; Kendall, C.; Shepherd, N.; Crow, P.; Barr, H. Near-Infrared Raman Spectroscopy for the Classification of Epithelial Pre-Cancers and Cancers. *J. Raman Spectrosc.* **2002**, *33*, 564−573.
(50) Salman, A.; Shufan, E.; Zeiri, L.; Huleihel, M. Characterization and Detection of Vero Cells Infected with Herpes Simplex Virus Type 1 using Raman Spectroscopy and Advanced Statistical Methods. *Methods* **2014**, *68*, 364−370.
(51) Gonzalez-Navajas, J. M.; Lee, J.; David, M.; Raz, E. Immunomodulatory Functions of Type I Interferons. *Nat. Rev. Immunol.* **2012**, *12*, 125−135.
(52) Gomez, C. R.; Boehmer, E. D.; Kovacs, E. J. The Aging Innate Immune System. *Curr. Opin. Immunol.* **2005**, *17*, 457−462.

DOI: 10.1021/acsanm.8b00779
ACS Appl. Nano Mater. 2018, 1, 5451−5459

(53) Schoggins, J. W.; Rice, C. M. Interferon-Stimulated Genes and Their Antiviral Effector Functions. *Curr. Opin. Virol.* **2011**, *1*, 519−525.
(54) Yu, Y.; Huang, X.; Liu, J.; Zhang, J.; Hu, Y.; Yang, Y.; Huang, Y.; Qin, Q. Fish TRIM32 Functions as a Critical Antiviral Molecule against Iridovirus and Nodavirus. *Fish Shellfish Immunol.* **2017**, *60*, 33−43.

DOI: 10.1021/acsanm.8b00779
ACS Appl. Nano Mater. 2018, 1, 5451−5459